v. 1.2, *Bull. Seism. Soc. Am.*, in press

Some Notes on Phase Derivatives and Simulating Strong Ground Motions

David M. Boore

Abstract

Phase derivatives can be used to compute instantaneous frequency and envelope delay (also known as group delay). Envelope delay, in the guise of phase differences, has been used by engineers in the simulation of strong ground motion, particularly as a way of controlling the duration of motion. Simulations using the stochastic method, in which duration is a simple function of source duration and a path-dependent duration, possess envelope delay properties similar to those from simulations based on phase differences. Envelope delay provides a way of extending the standard stochastic method to produce nonstationary frequency content, as produced by ground motions containing surface waves.

Introduction

For many years, seismologists have used the derivative of the phase spectrum of ground motion to compute group velocities and to simulate waveforms of dispersed waves (e.g., Aki, 1960 [see also Aki and Richards, 2002, problem 7.8]; Dziewonski *et al.*, 1969; Dziewonski and Hales, 1972). The use of group velocity to determine the relative arrivals of motion at different frequencies for multiple modes has been used by Trifunac and colleagues (e.g., Trifunac, 1971, and Wong and Trifunac, 1979) to simulate strong ground motion. In the engineering literature a number of papers have appeared in which "phase differences" play a central role in simulating earthquake ground motions (e.g., Ohsaki, 1979; Ohsaki *et al.*, 1984; Sawada, 1984; Thráinsson *et al.*, 2000; Shrikhande and Gupta, 2001; Montaldo *et al.*, 2002; Thráinsson and Kiremidjian, 2002), but aside from a scalar factor involving the frequency increment, these "phase differences" are nothing more than a

finite-difference approximation of the derivative of the phase with respect to frequency, and thus are an approximation of the group delays, well known in studies of dispersed waves (e.g., Udias, 1999). This paper has several purposes: to acquaint engineers with work of seismologists involving group delays and vice versa, and to introduce an extension of the widely-used stochastic method for simulating strong-ground motions (Boore, 2003) that will produce simulated motions with nonstationary frequency content, such as produced by basin waves (e.g., Boore, 1999; Joyner, 2000). This extension uses frequency-dependent phase derivatives.

Because I will be using the phase derivative of records that are not clearly dispersive, I will henceforth call the derivative of phase with respect to frequency the *envelope delay*, a term sometimes found in the electrical engineering literature. There are several advantages to using the envelope delay rather than phase differences. The envelope delay has units of time, and it has a natural physical interpretation that makes it clear why the phase differences are not random, even though the phases may appear to be so. In addition, by using Fourier transforms it is easy to compute the envelope delay without first unwrapping the phase and then using finite difference approximations for the derivative. The same procedure can be used to compute the instantaneous frequency of a time series without unwrapping the phase. This can be useful in identifying spikes in records and in assessing nonstationarity of the ground motion. The paper begins with the equations for computing phase derivatives, followed by a section showing examples of using the derivatives for recorded and simulated ground motions, and concludes with the extension to the stochastic method mentioned above.

Theory

Because phase derivatives appear in different contexts in this paper, the derivation here considers a generalized Fourier transform pair:

$$h(\eta) = \int_{-\infty}^{\infty} H(\xi) e^{-i2\pi\xi\eta}\, d\xi \tag{1a}$$

$$H(\xi) = \int_{-\infty}^{\infty} h(\eta) e^{i2\pi\xi\eta}\, d\eta. \tag{1b}$$

$h(\eta)$ and $H(\xi)$ are complex variables and can be written in terms of their amplitude and phase. (Note that a scaling factor involving 2π is not needed because the factor of 2π has been separated out from the integration variables— in more familiar terms, I am using frequency rather than angular frequency in the transform pair [Press *et al.*, 1992, pp. 490-491].) To simplify notation, in this paper I will work only with $H(\xi)$ written in this way:

$$H(\xi) = A(\xi)e^{i\phi(\xi)}. \tag{2}$$

Obtaining the amplitude $A(\xi)$ and phase $\phi(\xi)$ is straightforward, e.g., by computing the Fast Fourier Transform ($H(\xi)$) of $h(\eta)$, from which

$$A(\xi) = \sqrt{\Re(H)^2 + \Im(H)^2} \tag{3}$$

and

$$\phi(\xi) = \arctan(\Im(H)/\Re(H)), \tag{4}$$

where "$\Re(H)$" and "$\Im(H)$" are the real and imaginary parts of the complex variable H, respectively.

Of particular interest in this paper is $d\phi(\xi)/d\xi$. There are two situations in which this arises: envelope delay and instantaneous frequency. Details concerning each are in the following sections.

Because the phase given by equation (4) is wrapped between $-\pi$ and π, a straightforward finite-difference computation of the phase derivative first requires unwrapping the phase— not necessarily easy to do (Shatilo, 1992). A useful way to compute the phase derivative that does not require unwrapping the phase starts with taking the logarithm of equation (2) (Claerbout, 1992):

$$\ln H(\xi) = \ln A(\xi) + i\phi(\xi). \tag{5}$$

Taking the derivative with respect to ξ then gives

$$\frac{d\phi}{d\xi} = \Im(\frac{1}{H}\frac{dH}{d\xi}). \tag{6}$$

Differentiating equation (1b), it is easy to show that

$$dH(\xi)/d\xi = i2\pi G(\xi) = i2\pi[\Re(G) + i\Im(G)], \tag{7}$$

where $G(\xi)$ is the Fourier transform of $\eta h(\eta)$:

$$G(\xi) = \int_{-\infty}^{\infty} \eta h(\eta) \exp i2\pi\xi\eta d\eta. \tag{8}$$

Combining equations (6) and (7) gives

$$\frac{d\phi}{d\xi} = 2\pi[\Re(H)\Re(G) + \Im(H)\Im(G)]/A^2. \tag{9}$$

This gives the phase derivative of ϕ in terms of the Fourier transform of $h(\eta)$ and $\eta h(\eta)$, with no explicit derivatives needed (Stoffa *et al.*, 1974, eq. 34). The derivative given by equation (9) can be poorly behaved for values of ξ for which $A(\xi)$ becomes small. This is particularly a problem when $A(\xi)$ represents the envelope of a time series, and $d\phi/d\xi$ is the instantaneous frequency. In such cases it is useful to smooth the denominator and the numerator separately before taking the ratio in equation (9). A simple triangular weighting function works well for smoothing.

Note that any operation on $H(\xi)$ that leaves the ξ-dependence of the phase ϕ unchanged will not alter the phase derivative. As will be made clear later, this means that the envelope delay will be the same regardless of whether the time series represents acceleration, velocity, or displacement, because their phases differ by frequency-independent increments of 90°. The instantaneous frequency, however, is given by the time derivative of the phase, and the time dependence of the phase, and thus the instantaneous frequency, will depend on whether the time series represents acceleration, velocity, or displacement.

Data Used in Examples

To illustrate envelope delay and instantaneous frequency, I consider two recorded ground motions, one with relatively long-period surface waves that arrive after the body

waves, and one for which most of the energy content occurs in the same time window (the record is that used by Thráinsson and Kiremidjian, 2002, to illustrate some properties of phase differences). To see the relative arrival times of the different parts of the spectrum, it is best to plot a series of band-pass filtered motions. Instead, I use acceleration, velocity, and displacement traces as familiar surrogates for band-pass filtered motions. The results for the two recordings are shown in Figure 1. Note that the overall waveshapes for the Santa Cruz recording are rather similar for acceleration, velocity, and displacement, in distinct contrast to the waveshapes of the S3E recordings. The long-period late arrivals on the S3E record are surface waves that have traversed the Los Angeles basin (Boore, 1999).

Envelope and Instantaneous Frequency

Starting with a time series $y(t)$, form the complex time series $y_c(t)$

$$y_c(t) = y(t) - i\tilde{y}(t), \tag{10}$$

where $\tilde{y}(t)$ is the Hilbert transform of $y(t)$ ($y_c(t)$ is sometimes called the "analytic signal"). The transform $Y_c(f)$ of $y_c(t)$ is given most conveniently by

$$Y_c(f) = \begin{cases} 0.0, & f < 0.0 \quad (11a) \\ 2Y(f), & f \geq 0.0 \quad (11b) \end{cases}$$

where $Y(f)$ is the Fourier transform of y (Mitra, 2001, p. 794). Then use the mapping

$$h(\eta) \rightarrow Y_c(f) \tag{12a}$$

$$H(\xi) \rightarrow y_c(t) \tag{12b}$$

and the mapping of η and ξ to time and frequency

$$\xi \rightarrow t, \eta \rightarrow f.$$

The envelope of $y(t)$ is given by the envelope of the amplitude of H; this is

$$A(t) = \sqrt{y(t)^2 + y_c(t)^2}. \tag{13}$$

The derivative of the phase is used in the equation

$$f_I(t) = \frac{1}{2\pi}\frac{d\phi}{dt} \tag{14}$$

to give the time-dependent instantaneous frequency f_I (Farnbach, 1975, Taner *et al.*, 1979; Kanasewich, 1981; Bracewell, 1999). The phase used to compute the instantaneous frequency is given by

$$\phi(t) = -\arctan \tilde{y}(t)/y(t). \tag{15}$$

The time dependence of the phase, and thus $f_I(t)$, will depend on whether $y(t)$ represents acceleration, velocity, or displacement.

Examples of the envelope of a time series are shown in Figure 1 and the instantaneous frequencies are shown in Figure 2. For the S3E recording the instantaneous frequency shows a decrease with time, and as predicted, depends on the type of motion for which it is computed. I have not found instantaneous frequency to be a very useful quantity, although it has been used occasionally in seismology (e.g., Levshin *et al.*, 1992).

Envelope Delay

This paper is primarily concerned with the envelope delay because of its use in simulating strong ground motions. If $y(t)$ is a time series, use the following mapping:

$$h(\eta) \rightarrow y(t) \tag{16a}$$

$$H(\xi) \rightarrow Y(f) \tag{16b}$$

and

$$\eta \rightarrow t, \xi \rightarrow f.$$

(Since h and H are generalized variables, I did not have to switch the mapping of η and ξ to t and f compared to that used for instantaneous frequency; I changed the mapping, however, because I wanted to use only one equation — equation (2) — relating a complex variable and amplitude and phase.) With this mapping,

$$t_e(f) = \frac{1}{2\pi}\frac{d\phi}{df} \tag{17}$$

where, in the context of dispersive wave propagation (but also useful in general, as shown in this note), t_e is the frequency-dependent envelope delay (Kanasewich, 1981; Scherbaum, 2001, p. 190 [but with a minus sign because of his definition of the Fourier spectrum of $y(t)$]).

The envelope delay as a function of frequency for the two example acceleration records are shown in Figure 3. (In this and almost all other plots of envelope delay, I plot envelope delay on the abscissa even though it is the dependent variable; I do this to facilitate comparison with ground-motion time series, for which time is plotted on the abscissa.) The envelope delays clearly show the difference in the relative arrival times of different frequencies. The envelope delay for the Santa Cruz recording of the 1989 Loma Prieta earthquake is relatively insensitive to frequency (with a tendency for higher frequencies to arrive several seconds earlier than low frequencies), and the majority of the envelope delay values occur near 9 sec, which corresponds to the time of the peak in the envelope of the ground motion. (If the time series had been shifted in time, the envelope delay values would have been shifted by the same amount.) The envelope delays for the S3E recording indicate a strong nonstationarity in frequency content for frequencies less than about 5 Hz, with the lower frequencies arriving later than the higher frequencies; this is consistent with the displacement waveform shown in Figure 1. The centroid time of the energy at a particular frequency is related to the mean value of the envelope delay at that frequency, but the overall time-extent of the motion is determined by the statistical distribution of the envelope delay about the mean value.

The envelope delay for S3E shown in Figure 3 was computed from the acceleration time series and shows a strongly nonstationary frequency content, even though this nonstationarity is not particularly evident in the acceleration time series. This is consistent with theoretical expectations. To make the point empirically, envelope delays computed from the acceleration, velocity, and displacement traces for the S3E recording are shown in Figure 4. The delays are almost identical.

In addition to analysis of dispersion and the simulation of strong motion, envelope

delay has been used to aid in choosing corner frequencies of low-cut filters used in processing strong-motion accelerograms (N. Abrahamson, written. commun., 1993). Digitizing noise will dominate the signal at long periods, and this will show up as a shift of the envelope delay at low frequencies to smaller values (earlier arrivals, corresponding to amplification of the noise before the arrival of the seismic energy) and increased scatter in the delays as the filter frequency is decreased.

The Relation Between Probability Distribution of Envelope Delay and Waveform Shape and Duration

Ohsaki (1979) made the qualitative observation that the shape of the envelope of an acceleration time series and the probability distribution function (*pdf*) of phase differences are similar, and furthermore that the distribution of the phase differences appeared to be similar in shape to a normal distribution. Nigam (1982, 1984) derived an analytic expression for the distribution of the phase difference of a random process corresponding to Gaussian white noise multiplied by a time-domain shaping function; Nigam remarked that the distribution is not normal. (The equation for the distribution in Nigam, 1982, differs from that in Nigam, 1984 — the later equation predicts a bimodal distribution, but my simulations show that it is incorrect, and that the earlier equation is correct.) Other authors have studied phase differences as a means of characterizing and simulating ground motions (e.g., Ohsaki *et al.*, 1984; Sawada, 1984; Thráinsson *et al.*, 2000; Shrikhande and Gupta, 2001; Montaldo *et al.*, 2002; Thráinsson and Kiremidjian, 2002). Liao and Jin (1995) explicitly use the derivative of the phase, rather than phase difference. Here I use simulations to investigate Ohsaki's observation, using envelope delays rather than phase differences (another reason to use envelope delays rather than phase differences is that the independent variable of the probability distribution is time rather than radians, and plots of the *pdf* can be compared directly to the envelope of the times series).

The simulation method is the widely-used stochastic method (see Boore, 2003, for a review). The stochastic method represents possibly complex physics with simple functional forms, attempting to account for the essence of the physics; it combines seismological theory

and the engineering notion that ground motion is a random process. Of particular interest in this paper is the duration of the random process, given in the stochastic method by the addition of the source duration and an empirically derived duration related to distance traveled between the source and the site. This results in a nonstationary random process in the sense that the process is of limited duration, but the frequency content of the motion is stationary. In a later section I describe a way of using envelope delay to produce nonstationary frequency content in the context of the stochastic method.

The stochastic method does not make explicit use of the statistical properties of the envelope delay, as does the simulation method of Thráinsson *et al.* (2000), Montaldo *et al.* (2002), and Thráinsson and Kiremidjian (2002). In particular, those authors use empirical distributions of the phase differences as a function of frequency and as a function of the Fourier amplitude spectra. I thought it would be interesting to see if the distributions of the envelope delay from the stochastic-method simulations are similar to those from data. I will compare the Santa Cruz recording of the 1989 Loma Prieta, California, earthquake and my simulations using a generic model for a coastal California rock site (file "wr032496.dat" in Boore, 2000). The simulations were computed for a magnitude of 6.9 and a distance of 10 km; no attempt was made to adjust the parameters of the model to match the data. Two envelope functions were used in the simulations: a box window and a more realistic shaped window made up of time raised to a power multiplied by an exponential decay (see Boore, 2000, for details). The envelope delay is plotted against frequency in Figure 5 for the first of a suite of simulations. Also plotted in the figure is the envelope delay for the Santa Cruz recording. The distributions of envelope delays are qualitatively similar, except for the differences in the mean values (which are dependent on the arbitrary origin time of each record and have nothing fundamental to do with the waveforms of the ground motion). The comparison of the data used to obtain the amplitude information by Thráinsson and colleagues is shown in Figure 6; again, there is good qualitative agreement between the simulations and the data. By using envelope delay rather than phase differences, it is easier to understand the character of the plot shown in Figure 6: the largest amplitudes occur over a relatively narrow range of time, whereas the smaller motions (e.g., coda waves) are

spread out over a longer portion of time. This leads to a spreading of the distribution of envelope delay as the amplitude decreases.

Knowing that the stochastic method produces envelope delay properties in good qualitative agreement with those from data, I simulated 99 acceleration time series for both the box and the shaped windows. The top two panels in Figure 7 show the time series for the first of the 99 simulations (in gray), along with the mean envelope of the simulations. Also shown is the probability distribution of the envelope delay, using the formula from Nigam (1982). (A technical aside: Nigam's formula is based on a model in which filtered white noise is windowed, but Şafak and Boore, 1988, show that this procedure — commonly used by engineers — distorts the low-frequency portion of the spectrum. The stochastic method simulations used in Figure 7 do not contain this distortion, and therefore the models of the random process assumed by Nigam, 1982, and used in the stochastic method simulations are not strictly comparable; the difference, however is not important for the comparison shown in Figure 7.) From this figure it is clear that the probability distribution of the envelope delay has only a passing similarity to the average envelope of the acceleration time series, and that the *pdf* for both the box and the shaped window are very similar. The bottom two plots compare the histograms of the envelope delay with the *pdf* from Nigam; this comparison simply serves as a qualitative check of his equation (I made the decision that a more quantitative comparison was not warranted, because no further use will be made of the theoretical *pdf*).

Using Envelope Delay to Account for Time-Dependent Frequency Content in Stochastic-Method Simulations

The standard stochastic method does not account for nonstationarity of frequency content of the ground motion, which can be important in some situations, particularly when basin waves are present (as they are for the S3E recording of the 1990 Upland earthquake, used as one of the two examples in this paper). Basin waves can significantly increase the amplitude at long periods, as well as lead to increased durations of these motions. The increase of motions at long periods is shown in Figure 8, which compares

response spectra with and without the basin waves, with predictions based on the standard stochastic method and with empirical ground-motion predictions. Frequency-dependent envelope delay provides a way to extend the stochastic method to allow for nonstationarity of the frequency content. This section illustrates an initial attempt to do this. There are two parts to the extension: 1) account for the increased duration of the longer period waves, and 2) account for the increased amplification of the basin waves.

I accounted for the increased duration by first fitting a simple function to the envelope delay (the derivative of phase with respect to frequency), and then integrating this functional form with a constant of integration chosen to give zero incremental phase at high frequencies. I applied this phase correction to the time series simulated in the standard way for the stochastic method (Boore, 1983, 2003). After plotting the envelope delay for the S3E record in various ways, I found that using a log axis for the abscissa suggested that a simple straightline fit of the envelope delay as a function of log frequency was a good representation of the observed envelope delays (Figure 9).

As shown by the relatively good agreement between the stochastic model simulations and the response spectra computed without the basin waves (Figure 8), the amplification function used in the simulation of the motion without basin waves was reasonable. To account for the basin waves, I computed the ratio of the Fourier spectra of the complete S3E record and the portion of the record up to 50 s (effectively removing the basin waves). The individual spectra and the spectral ratio are shown in the upper plot Figure 10. I smoothed the ratio slightly, and approximated the ratio by a series of connected line segments (these are also shown in the upper part of Figure 10). The amplification without the basin waves (as used in the AB98 model simulations shown in Figure 8), the basin wave amplification, and the combined amplification are shown in the lower plot of Figure 10. In addition to the amplification, the simulation included a diminution function given by path-dependent attenuation and the path-independent attenuation function $\exp(-\pi\kappa_0 f)$, where $\kappa_0 = 0.0516$ (see Boore, 1999, for details).

By combining the additional amplifications and the phase corrections, it is possible

to include the basin waves by making simple modifications to the software that produces stochastic-method time-domain simulations (e.g., SMSIM; see Boore, 2000, 2002). The results of doing so are shown in Figure 11, which compares the predicted motions at S3E (74 km from a moment magnitude 5.6 earthquake) without basin waves, with the basin wave amplifications, with the basin wave amplifications and the nonstationary frequency content, and the observations. As this is only an illustration of a concept, I am not trying to match exactly the observed waveforms (this could undoubtedly be done by varying the input parameters). The general character of the duration and amplitude of the basin waves has been captured by this simple modification to the standard stochastic method. The modification could also be used by other simulation methods for which the usual method results in stationary frequency content (e.g., FINSIM, Beresnev and Atkinson, 1998).

The simulations in Figure 11 are clearly specific for the S3E record. An important question is whether the necessary amplification and duration properties can be determined for an arbitrary site within a basin. This question is beyond the scope of this paper, but duration should be related to group velocities of surface waves propagating in the basin, and thus is potentially predictable. On the other hand, a number of studies of basin amplification find that amplification depends on source location (some of these studies have been reviewed in Field and the SCEC Phase III Working Group, 2000). Unless some way is found to capture the essence of this amplification without doing a complete finite-difference calculation, this may make it difficult to account for basin response at specific source and site pairs using the simple extension to the stochastic method proposed here.

Discussion and Conclusions

Phase derivatives are useful in determining instantaneous frequency and the envelope delay of time series. These derivatives can be computed using Fourier transforms, without unwrapping the phase and forming finite-difference approximations. As illustrated by ground-motion recordings with and without basin waves, the envelope delay contains information about the duration of ground motion, including nonstationary frequency content.

The statistical properties of envelope delay as a function of frequency and amplitude have been used in simulations of ground motion (e.g., Thráinsson and Kiremidjian, 2002). I find that the envelope delays for simulations using the stochastic method, in which duration is given by the addition of a simple distance-dependent duration and the source duration, and amplitude is determined by standard seismological models of Fourier spectra of the source, path, and site, have statistical properties qualitatively similar to those from data. Envelope delay has the advantage over phase differences that it can be interpreted more directly in terms of the duration and waveforms of ground motion, and in addition, can be used to extend stochastic simulations of ground motion to account for nonstationary frequency content.

Acknowledgments

I thank Norm Abrahamson for first acquainting me with the algorithm for obtaining the phase derivative without unwrapping the phase, Bob Herrmann for several conversations, Anne Kiremidjian for copies of her papers, and Erdal Şafak, Chris Stephens, and Frank Scherbaum for reviews of the paper.

References

Abrahamson, N.A. and K.M. Shedlock (1997). Overview, *Seism. Res. Lett.* **68**, 9–23.

Abrahamson, N.A. and W.J. Silva (1997). Empirical response spectral attenuation relations for shallow crustal earthquakes, *Seism. Res. Lett.* **68**, 94–127.

Aki, K. (1960). Study of earthquake mechanism by a method of phase equalization applied to Rayleigh and Love waves, *J. Geophys. Res.* **65**, 729–740.

Aki, K. and P.G. Richards (2002). *Quantitative Seismology Theory and Methods: Second Edition*, 700 p., University Science Books, Sausalito, California.

Atkinson, G.M. and D.M. Boore (1998). Evaluation of models for earthquake source spectra in eastern North America, *Bull. Seism. Soc. Am.* **88**, 917–934.

Beresnev, I.A. and G.M. Atkinson (1998). FINSIM— a FORTRAN program for simulating stochastic acceleration time histories from finite faults, *Seism. Res. Lett.* **69**, 27–32.

Boore, D.M. (1983). Stochastic simulation of high-frequency ground motions based on seismological models of the radiated spectra, *Bull. Seism. Soc. Am.* **73**, 1865–1894.

Boore, D.M. (1999). Basin waves on a seafloor recording of the 1990 Upland, California, earthquake: Implications for ground motions from a larger earthquake, *Bull. Seism. Soc. Am.* **89**, 317–324.

Boore, D.M. (2000). SMSIM – Fortran programs for simulating ground motions from earthquakes: version 2.0 — A revision of OFR 96-80-A, *U.S. Geol. Surv. Open-File Rept. OF 00-509*, 55 pp.

Boore, D.M. (2002). SMSIM: Stochastic Method SIMulation of ground motion from earthquakes, in *IASPEI Centennial International Handbook of Earthquake and Engineering Seismology*, (P. Jennings, H. Kanamori, and W. Lee, Editors), Chapter 85.13, (in press).

Boore, D.M. (2003). Prediction of ground motion using the stochastic method, *Pure and Applied Geophy.* **160**, (in press).

Boore, D.M. and C.E. Smith (1999). Analysis of earthquake recordings obtained from the Seafloor Earthquake Measurement System (SEMS) instruments deployed off the coast of southern California, *Bull. Seism. Soc. Am.* **89**, 260–274.

Boore, D. M., W. B. Joyner, and T. E. Fumal (1997). Equations for estimating horizontal response spectra and peak acceleration from western North American earthquakes: A summary of recent work, *Seism. Res. Lett.* **68**, 128–153.

Bracewell, R.N. (1999). *The Fourier Transform & Its Applications*, McGraw-Hill, New York, New York, 640 pp.

Claerbout, J.F. (1992). *Earth Soundings Analysis: Processing Versus Inversion*, Blackwell Science, Inc.

Dziewonski, A., S. Bloch, and M. Landisman (1969). A technique for the analysis of transient seismic signals, *Bull. Seism. Soc. Am.* **59**, 427–444.

Dziewonski, A.M. and A.L. Hales (1972). Numerical analysis of dispersed seismic waves, Volume 11 - Seismology: Surface Waves and Earth Oscillations, in *Methods in Computational Physics*, B.A. Bolt (Editor), Academic Press, New York, 39–85.

Farnbach, J.S. (1975). The complex envelope in seismic signal analysis, *Bull. Seism. Soc. Am.* **65**, 951–962.

Field, E.H. and the SCEC Phase III Working Group (2000). Accounting for site effects in probabilistic seismic hazard analyses of southern California: Overview of the SCEC Phase III report, *Bull. Seism. Soc. Am.* **90**, S1–S31.

Joyner, W.B. (2000). Strong motion from surface waves in deep sedimentary basins, *Bull. Seism. Soc. Am.* **90**, S95–S112.

Kanasewich, E.R. (1981). *Time Sequence Analysis in Geophysics*, The University of Alberta Press, Edmonton, Alberta, Canada, 480 pp.

Levshin, A., L. Ratnikova, and J. Berger (1992). Peculiarities of surface-wave propagtion across central Eurasia, *Bull. Seism. Soc. Am.* **82**, 2464–2493.

Liao, Z.-P. and X. Jin (1995). A stochastic model of the Fourier phase of strong ground motion, *Acta Seismologica Sinica* **8**, 435–446.

Mitra, S.K. (2001). *Digital Signal Processing*, McGraw-Hill Irwin, New York, New York, 866 pp.

Montaldo, V., A.S. Kiremidjian, H. Thráinsson, and G. Zonno (2002). Simulation of the

Fourier phase spectrum for the generation of synthetic accelerograms, *J. Earthq. Eng.* , (submitted).

Nigam, N.C. (1982). Phase properties of a class of random processes, *Earthq. Eng. Struct. Dyn.* **10**, 711–717.

Nigam, N.C. (1984). Phase properties of earthquake ground acceleration records, *Proc. Eighth World Conf. Earthq. Eng.* **II**, Prentice-Hall, Inc. Englewood Cliffs, New Jersey, 549–556.

Ohsaki, Y. (1979). On the significance of phase content in earthquake ground motions, *Earthq. Eng. Struct. Dyn.* **7**, 427–439.

Ohsaki, Y., J. Kanda, R. Iwasaki, T. Masao, Y. Kitada, and K. Sakata (1984). Improved methods for generation of simulated earthquake ground motions, *Proc. Eighth World Conf. Earthq. Eng.* **II**, Prentice-Hall, Inc. Englewood Cliffs, New Jersey, 573–580.

Press, W.H., S.A. Teukolsky, W.T. Vetterling, and B.P. Flannery (1992). *Numerical Recipes in FORTRAN: The Art of Scientific Computing*, Cambridge University Press, Cambridge, England, 963 pp.

Şafak, E. and D.M. Boore (1988). On low-frequency errors of uniformly modulated filtered white-noise models for ground motions, *Earthq. Eng. Struct. Dyn.* **16**, 381–388.

Sawada, T. (1984). Application of phase differences to the analysis of nonstationarity of earthquake ground motion, *Proc. Eighth World Conf. Earthq. Eng.* **II**, Prentice-Hall, Inc. Englewood Cliffs, New Jersey, 557–564.

Scherbaum, F. (2001). *Of Poles and Zeros*, Kluwer Academic Publishers, Dordrecht, The Netherlands, 268 pp.

Shatilo, A.P. (1992). Seismic phase unwrapping: Methods, results, problems, *Geophysical Prospecting* **40**, 211–225.

Shrikhande, M. and V.K. Gupta (2001). On the characterisation of the phase spectrum for strong motion synthesis, *J. Earthq. Eng.* **5**, 465–482.

Stoffa, P.L., P. Buhl, and G.M. Bryan (1974). The application of homomorphic deconvolution to shallow-water marine seismology — Part I: Models, *Geophysics* **39**, 401–416.

Taner, M.T., F. Koehler, and R.E. Sheriff (1979). Complex seismic trace analysis, *Geophysics* **44**, 1041–1063.

Thráinsson, H. and A.S. Kiremidjian (2002). Simulation of digital earthquake accelerograms using the inverse Fourier transform, *Earthq. Eng. Struct. Dyn.* **31**, in press.

Thráinsson, H., A.S. Kiremidjian, and S.R. Winterstein (2000). Modeling of earthquake ground motion in the frequency domain, John A. Blume Center Report 134, Stanford University, Stanford, CA, 249 pp.

Tribolet, J.M. (1979). *Seismic Applications of Homomorphic Signal Processing*, Prentice-Hall, Englewood Cliffs, New Jersey, 195 pp.

Trifunac, M.D. (1971). A method for synthesizing realistic strong ground motion, *Bull. Seism. Soc. Am.* **61**, 1739–1753.

Udias, A. (1999). *Principles of Seismology*, Cambridge University Press, Cambridge, England, 475 p.

Wong, H.L. and M.D. Trifunac (1979). Generation of artificial strong motion accelerograms, *Earthq. Eng. Struct. Dyn.* **7**, 509–527.

Figure Captions

Figure 1. Acceleration, velocity, and displacement horizontal-component time series and envelopes (for the displacement) for the ocean bottom (S3E) recording of the 1990 Upland, California, **M** 5.6 earthquake (orientation of horizontal component unknown, low-cut filtered at 0.1 Hz: see Boore and Smith, 1999; Boore, 1999; data available from http://quake.usgs.gov/~boore) and for the U.C. Santa Cruz (Lick Lab.) recording of the 1989 Loma Prieta, California, **M** 6.9 earthquake (east-west component, low-cut filtered with a ramp from 0.05 to 0.1 Hz, data from the California Strong Motion Instrumentation Program, ftp://ftp.consrv.ca.gov/pub/dmg/csmip/LomaPrieta89/). r_{ep} and r_{jb} are epicentral and Joyner-Boore distances, respectively (see Abrahamson and Shedlock, 1997). Note the different time scales for the two recordings.

Figure 2. Instantaneous frequency (gray lines) for the Santa Cruz recording of the 1989 Loma Prieta, California, earthquake and the S3E recording of the 1990 Upland, California, earthquake. The ordinate labels for the instantaneous frequency are given on the right axes. The top two panels are for acceleration, and the same scaling has been used for instantaneous frequency in both panels. Note that the scaling for the instantaneous frequency differs for the acceleration, velocity, and displacement time series in the bottom three panels. The instantaneous frequency was smoothed with a triangular smoothing operator having a base width of 5 sec.

Figure 3. Frequency vs. envelope delay for acceleration for the two acceleration traces shown in Figure 1. Note the different scales for the envelope delay times, and the correspondence of the envelope delays with the times of ground shaking (as seen from Figure 1). In particular, note that the envelope delay for the S3E record shows a strong dependence on frequency, with lower frequencies corresponding to greater values of the envelope delay, as would be predicted from Figure 1. In contrast, the envelope delays for the Santa Cruz recording of the Loma Prieta earthquake show little frequency dependence, also as expected from the relative times of the envelopes of the acceleration, velocity, and displacements shown in Figure 1. The density of points along the ordinate is greater for the S3E recording than for the Santa Cruz recording (a factor of 4) because the S3E recording has a longer duration than the Santa Cruz recording, and therefore the interval between adjacent frequencies is smaller. The envelope delays were not smoothed.

Figure 4. Frequency vs. envelope delay for acceleration, velocity, and displacement time series for the S3E recording of the 1990 Upland, California, earthquake. As expected, the envelope delays are almost identical. The envelope delays were not smoothed.

Figure 5. Frequency vs. envelope delay for simulation 1 (see text), using box and shaped windows, and for comparison, the envelope delay from the Santa Cruz recording of the 1989 Loma Prieta, California, earthquake. The frequency interval between points is the same for each plot, as is the scaling of the abscissa. The envelope delays were not smoothed.

Figure 6. Envelope delay vs. amplitude for simulation 1 (see text), box and shaped windows, and for the Santa Cruz recording of the 1989 Loma Prieta, California, earthquake. The scalings of the abscissa and ordinate are the same for all plots. The envelope delays were not smoothed.

Figure 7. Probability density distributions (normalized to have unit area) of envelope delays from individual simulations, average of 99 simulations, and Nigam (1982) for box and shaped windows are shown in the bottom two graphs. Note the similarity of the probability density distributions for the two windows. The top two graphs show the acceleration time series from simulation 1 (see text), using box and shaped windows, as well as the average envelope from 99 simulations. Also shown in the top two graphs is the theoretical probability density distribution (right axis) from Nigam (1982).

Figure 8. Observed and predicted 5%-damped pseudo relative velocity response spectra (PSV) for the horizontal components of motion at station S3E from the 1990 Upland, California, earthquake. The solid lines are from the data: the thick and thin lines are the PSV from the whole record and from the S-wave portion of the record (the first 50 seconds of record shown in Figure 1), respectively. The spectra are the geometric mean of the spectra for the two horizontal components. The dashed lines are from empirical regression equations published by Abrahamson and Silva (1997) and Boore *et al.* (1997), and the dots are theoretical predictions assuming body-wave arrivals and the source model of Atkinson and Boore (1998) (AB98). (modified from Boore, 1999.)

Figure 9. Envelope delay for the recording of the 1990 Upland, California, earthquake at station S3E, with log axis for the abscissa. The straight lines were fit by eye and were used to represent the mean envelope delay for use in the stochastic modeling. The envelope delays were not smoothed.

Figure 10. (upper) Fourier amplitude spectra (FAS) of the acceleration recording of the 1990 Upland, California, earthquake at station S3E , smoothed over 0.01 Hz, for the complete record and the first 60 sec of the record (see Figure 1 for a plot of the acceleration time series) (gray lines), along with the computed spectral ratio and straightline approximation of the spectral ratio (black lines); (lower) amplification functions as used in the simulations with and without the basin waves, along with the basin-only amplifications.

Figure 11. Simulation using frequency-dependent correction to phase given by envelope delay of the 1990 Upland, California, earthquake recorded at station S3E, as well as the relative site response as discussed in the text. Shown are the acceleration, velocity, and displacement of the simulations (with and without basin amplification and envelope delay), and the observed motions at S3E from the 1990 Upland earthquake (74 km epicentral distance and **M** 5.6).

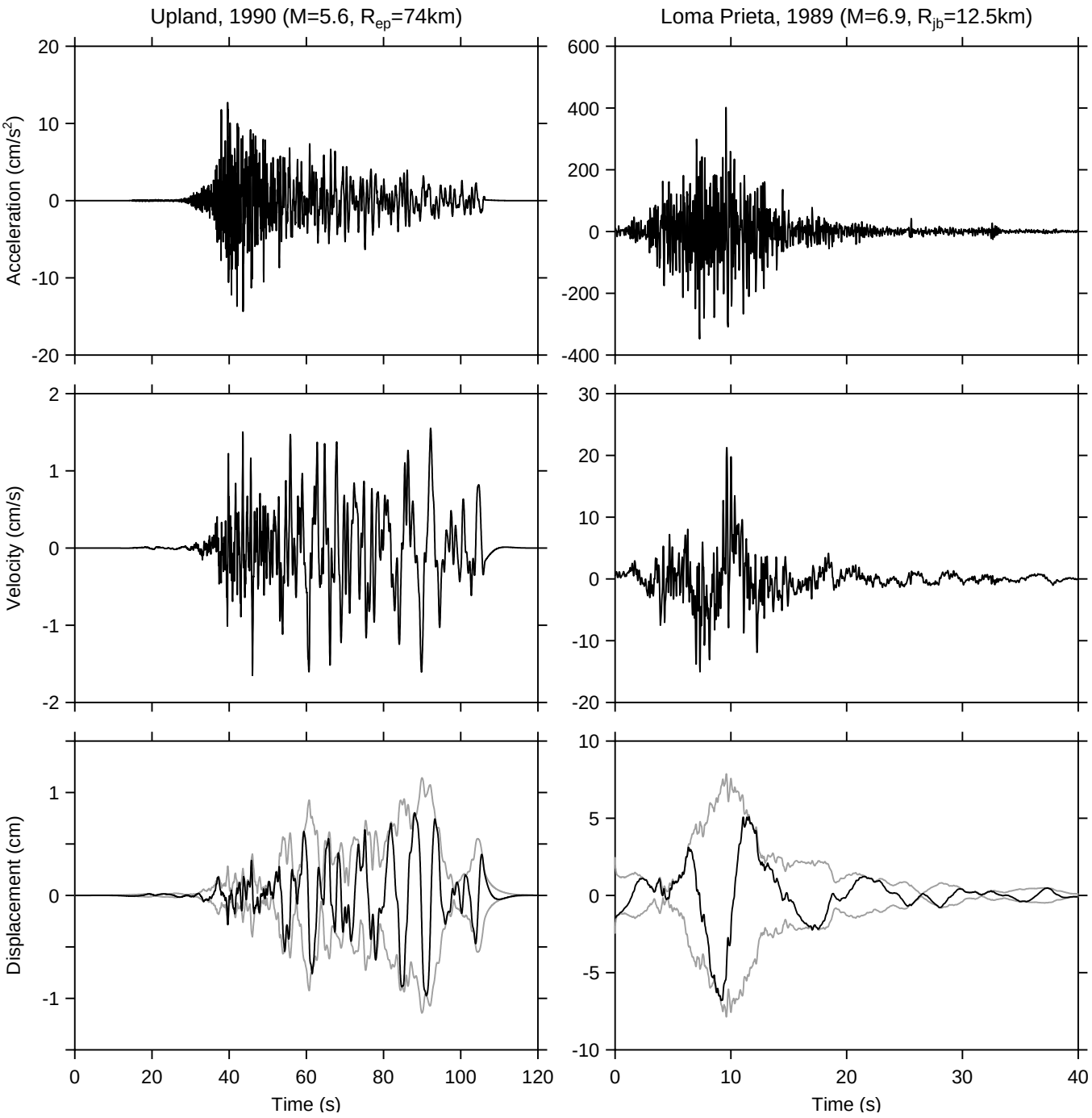

Figure 1. Acceleration, velocity, and displacement horizontal-component time series and envelopes (for the displacement) for the ocean bottom (S3E) recording of the 1990 Upland, California, **M** 5.6 earthquake (orientation of horizontal component unknown, low-cut filtered at 0.1 Hz: see Boore and Smith, 1999; Boore, 1999; data available from http://quake.usgs.gov/~boore) and for the U.C. Santa Cruz (Lick Lab.) recording of the 1989 Loma Prieta, California, **M** 6.9 earthquake (east-west component, low-cut filtered with a ramp from 0.05 to 0.1 Hz, data from the California Strong Motion Instrumentation Program, ftp://ftp.consrv.ca.gov/pub/dmg/csmip/LomaPrieta89/). r_{ep} and r_{jb} are epicentral and Joyner-Boore distances, respectively (see Abrahamson and Shedlock, 1997). Note the different time scales for the two recordings.

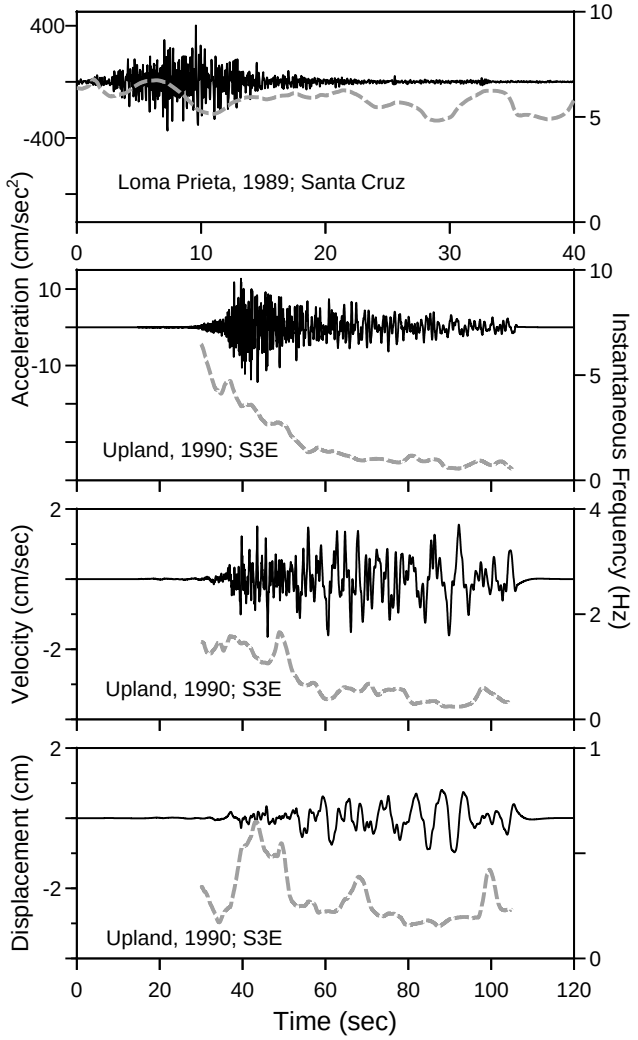

Figure 2. Instantaneous frequency (gray lines) for the Santa Cruz recording of the 1989 Loma Prieta, California, earthquake and the S3E recording of the 1990 Upland, California, earthquake. The ordinate labels for the instantaneous frequency are given on the right axes. The top two panels are for acceleration, and the same scaling has been used for instantaneous frequency in both panels. Note that the scaling for the instantaneous frequency differs for the acceleration, velocity, and displacement time series in the bottom three panels. The instantaneous frequency was smoothed with a triangular smoothing operator having a base width of 5 sec.

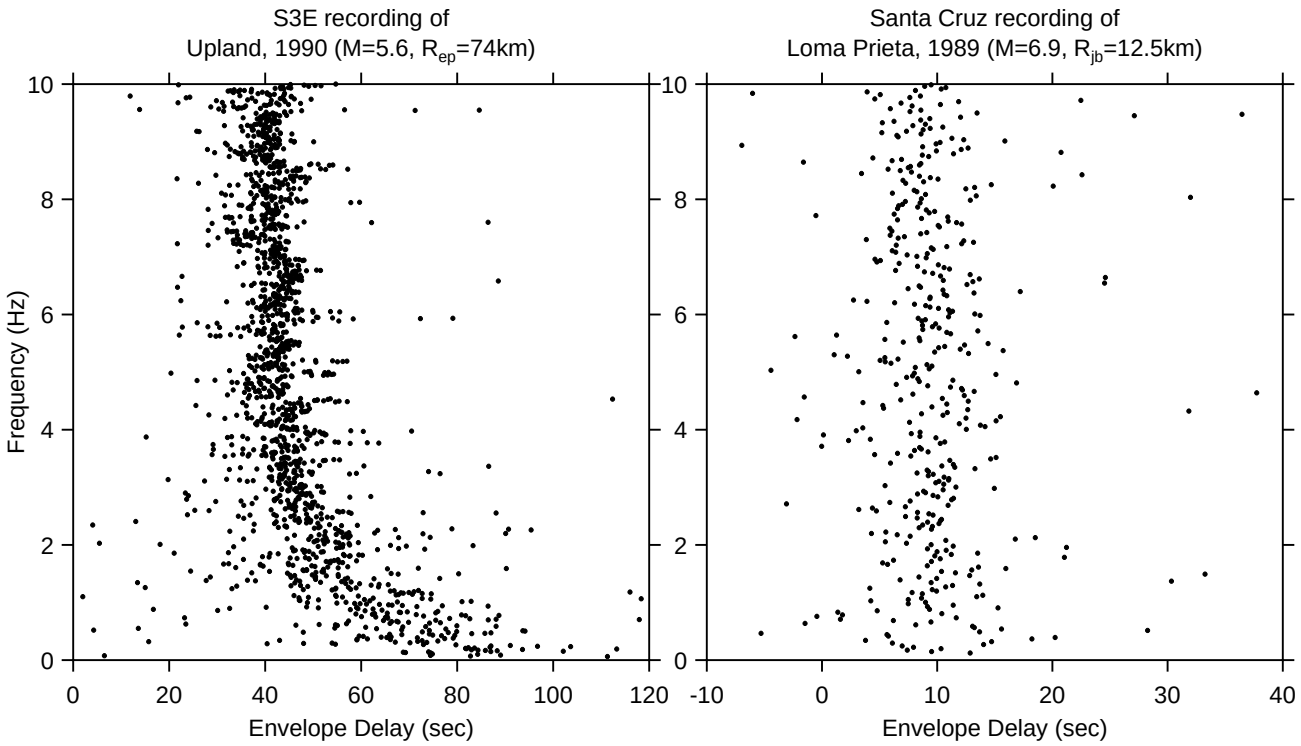

Figure 3. Frequency vs. envelope delay for acceleration for the two acceleration traces shown in Figure 1. Note the different scales for the envelope delay times, and the correspondence of the envelope delays with the times of ground shaking (as seen from Figure 1). In particular, note that the envelope delay for the S3E record shows a strong dependence on frequency, with lower frequencies corresponding to greater values of the envelope delay, as would be predicted from Figure 1. In contrast, the envelope delays for the Santa Cruz recording of the Loma Prieta earthquake show little frequency dependence, also as expected from the relative times of the envelopes of the acceleration, velocity, and displacements shown in Figure 1. The density of points along the ordinate is greater for the S3E recording than for the Santa Cruz recording (a factor of 4) because the S3E recording has a longer duration than the Santa Cruz recording, and therefore the interval between adjacent frequencies is smaller. The envelope delays were not smoothed.

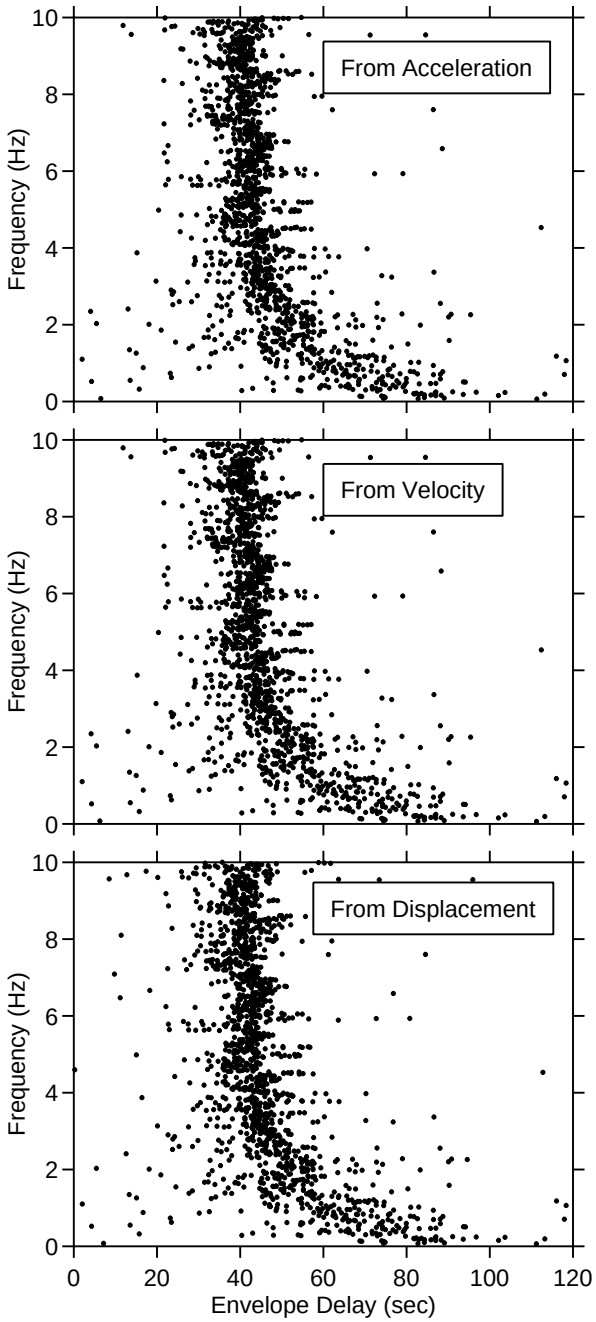

Figure 4. Frequency vs. envelope delay for acceleration, velocity, and displacement time series for the S3E recording of the 1990 Upland, California, earthquake. As expected, the envelope delays are almost identical. The envelope delays were not smoothed.

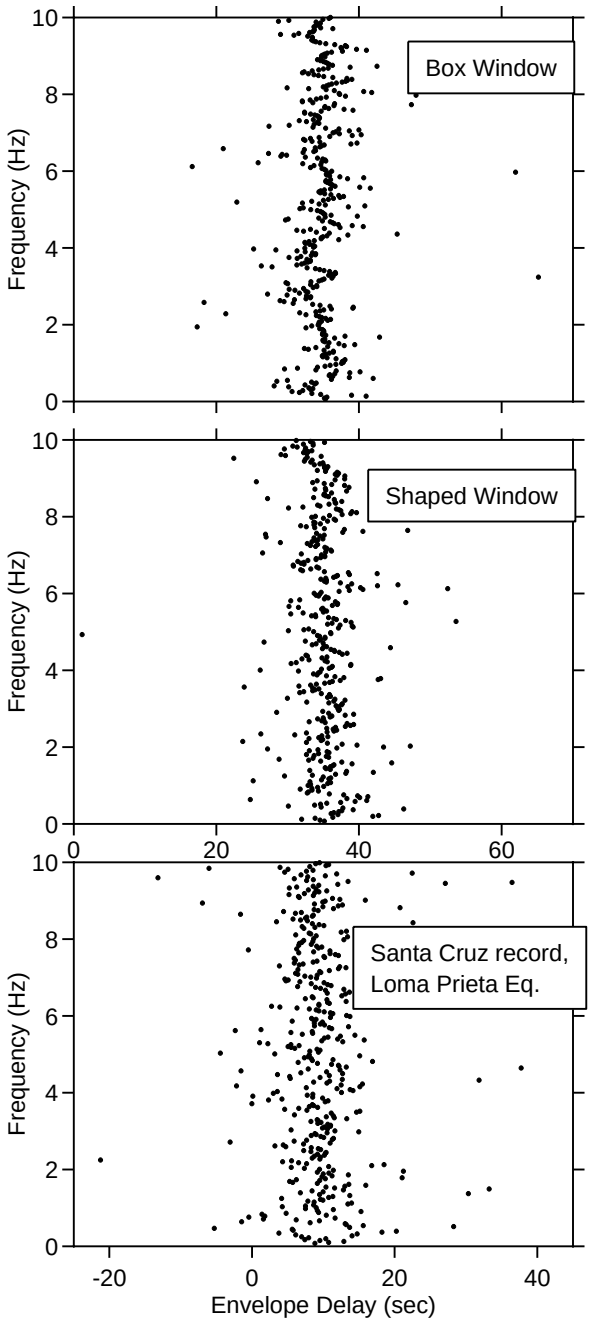

Figure 5. Frequency vs. envelope delay for simulation 1 (see text), using box and shaped windows, and for comparison, the envelope delay from the Santa Cruz recording of the 1989 Loma Prieta, California, earthquake. The frequency interval between points is the same for each plot, as is the scaling of the abscissa. The envelope delays were not smoothed.

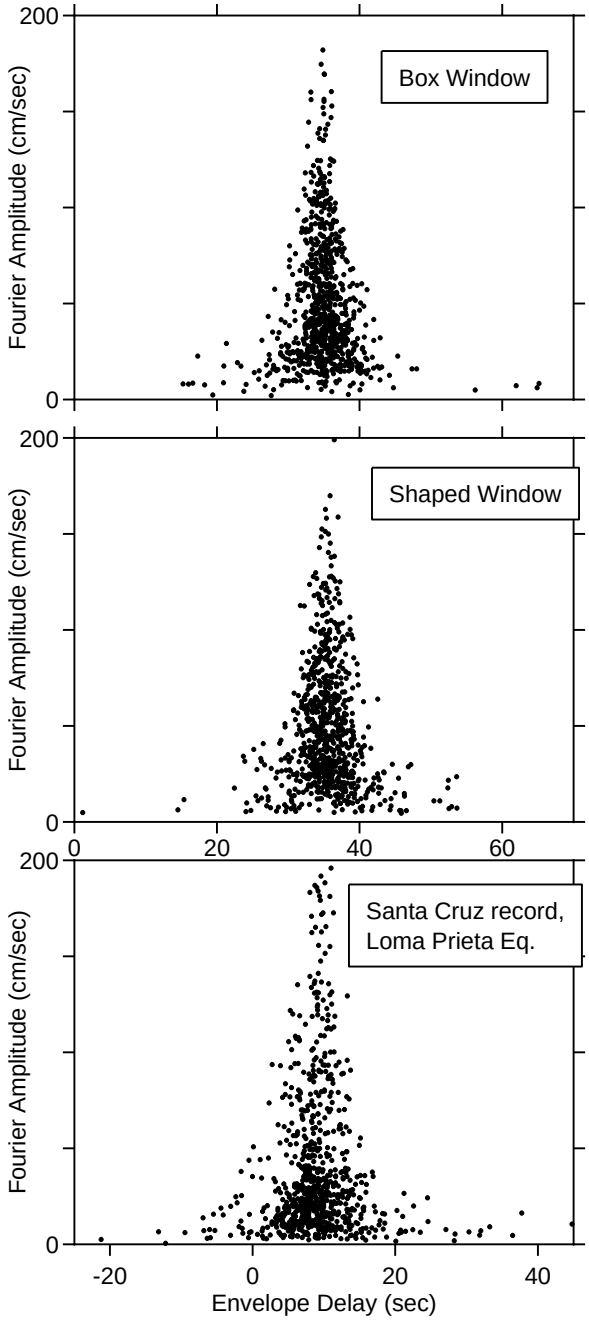

Figure 6. Envelope delay vs. amplitude for simulation 1 (see text), box and shaped windows, and for the Santa Cruz recording of the 1989 Loma Prieta, California, earthquake. The scalings of the abscissa and ordinate are the same for all plots. The envelope delays were not smoothed.

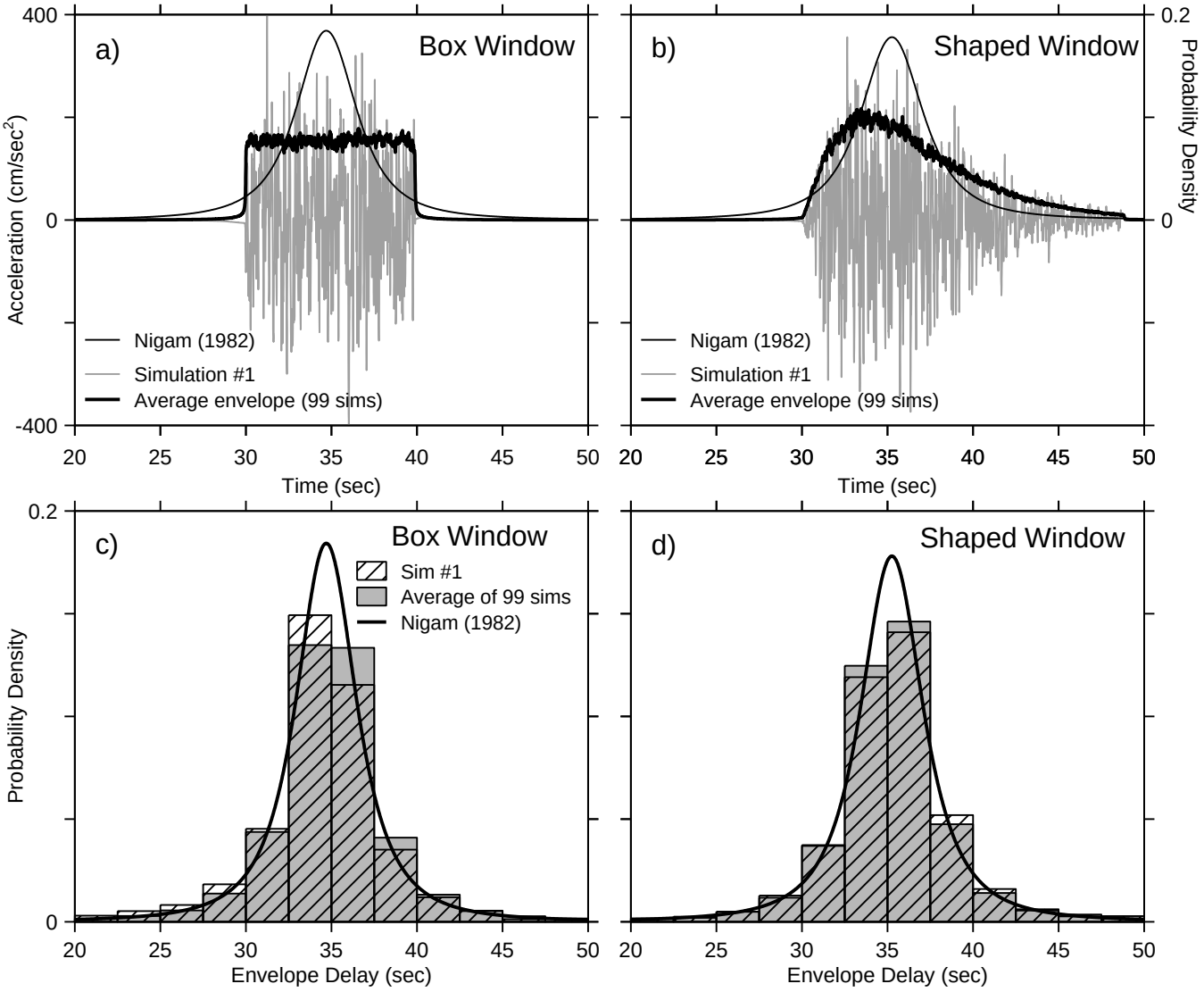

Figure 7. Probability density distributions (normalized to have unit area) of envelope delays from individual simulations, average of 99 simulations, and Nigam (1982) for box and shaped windows are shown in the bottom two graphs. Note the similarity of the probability density distributions for the two windows. The top two graphs show the acceleration time series from simulation 1 (see text), using box and shaped windows, as well as the average envelope from 99 simulations. Also shown in the top two graphs is the theoretical probability density distribution (right axis) from Nigam (1982).

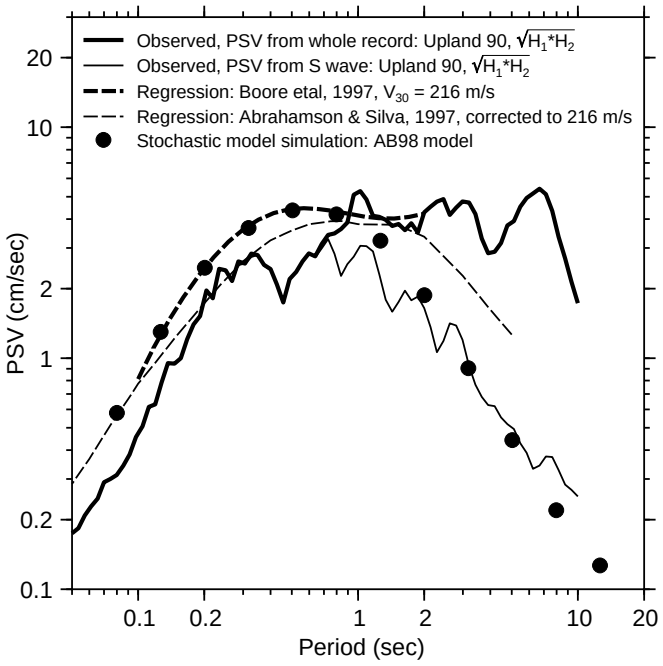

Figure 8. Observed and predicted 5%-damped pseudo relative velocity response spectra (PSV) for the horizontal components of motion at station S3E from the 1990 Upland, California, earthquake. The solid lines are from the data: the thick and thin lines are the PSV from the whole record and from the S-wave portion of the record (the first 50 seconds of record shown in Figure 1), respectively. The spectra are the geometric mean of the spectra for the two horizontal components. The dashed lines are from empirical regression equations published by Abrahamson and Silva (1997) and Boore *et al.* (1997), and the dots are theoretical predictions assuming body-wave arrivals and the source model of Atkinson and Boore (1998) (AB98). (modified from Boore, 1999.)

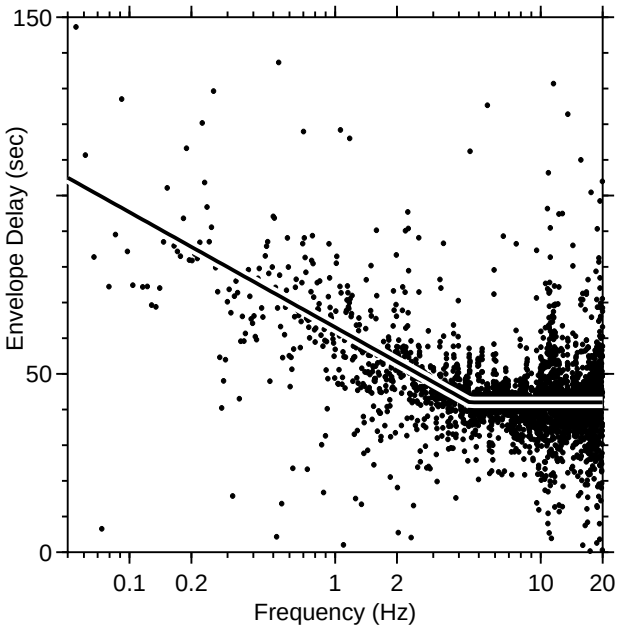

Figure 9. Envelope delay for the recording of the 1990 Upland, California, earthquake at station S3E, with log axis for the abscissa. The straight lines were fit by eye and were used to represent the mean envelope delay for use in the stochastic modeling. The envelope delays were not smoothed.

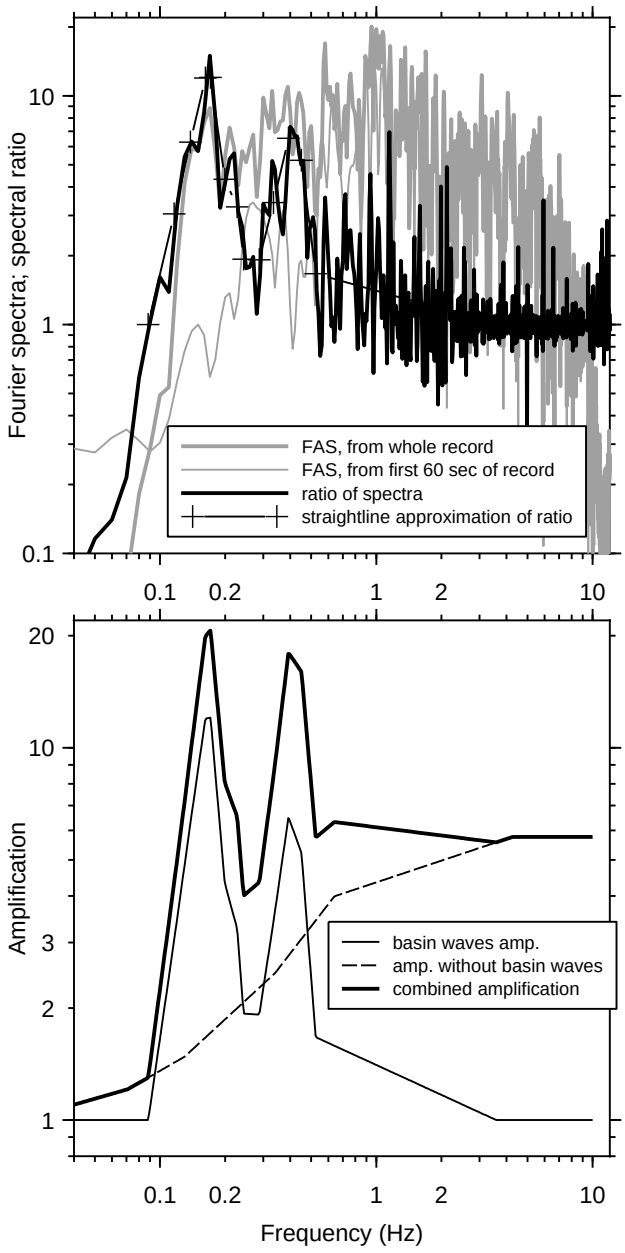

Figure 10. (upper) Fourier amplitude spectra (FAS) of the acceleration recording of the 1990 Upland, California, earthquake at station S3E , smoothed over 0.01 Hz, for the complete record and the first 60 sec of the record (see Figure 1 for a plot of the acceleration time series) (gray lines), along with the computed spectral ratio and straightline approximation of the spectral ratio (black lines); (lower) amplification functions as used in the simulations with and without the basin waves, along with the basin-only amplifications.

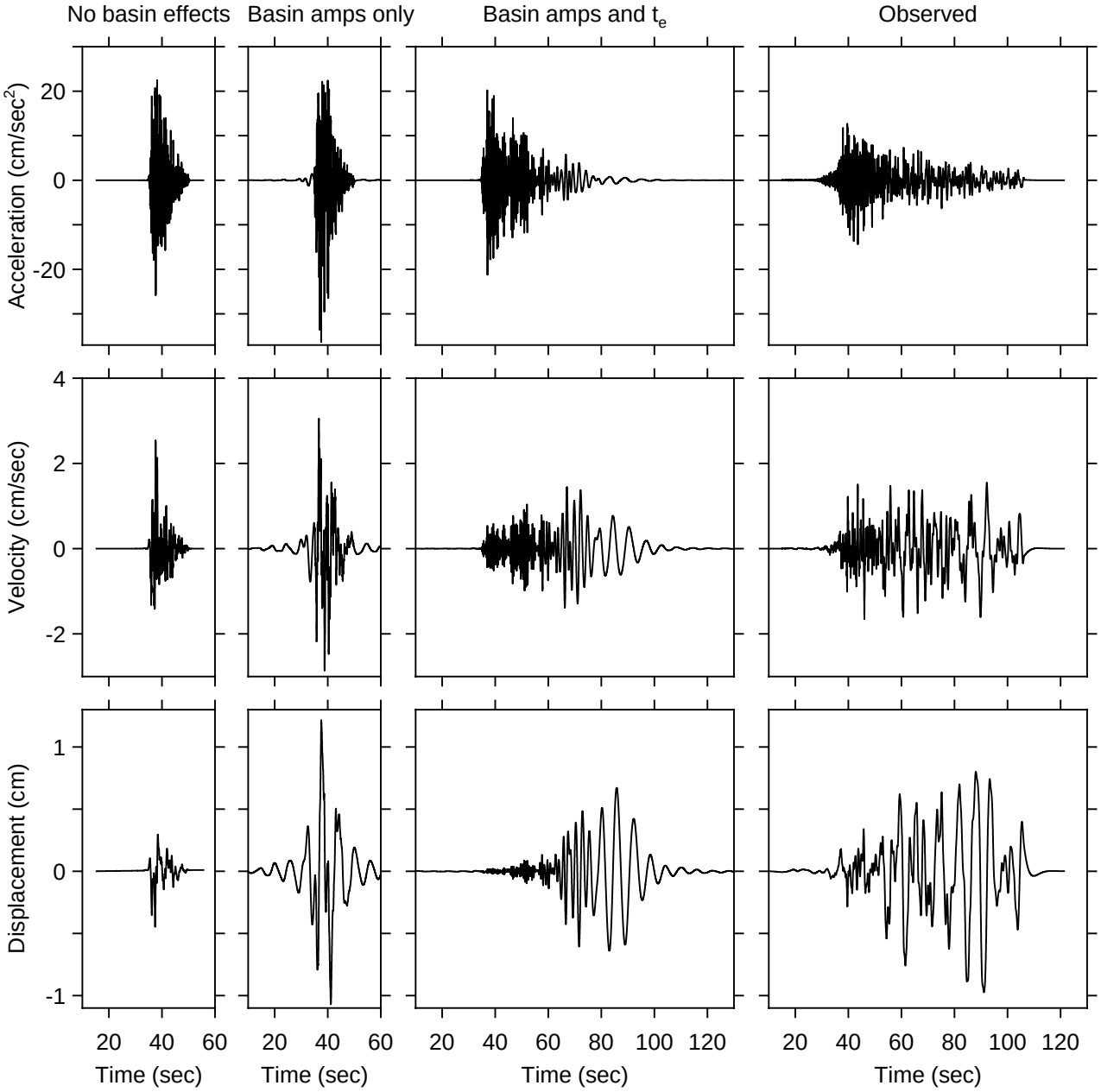

Figure 11. Simulation using frequency-dependent correction to phase given by envelope delay of the 1990 Upland, California, earthquake recorded at station S3E, as well as the relative site response as discussed in the text. Shown are the acceleration, velocity, and displacement of the simulations (with and without basin amplification and envelope delay), and the observed motions at S3E from the 1990 Upland earthquake (74 km epicentral distance and **M** 5.6).